Photochemically Generated Stable Cation Radical of Phenothiazine Aggregates in Mildly Acid Buffered Solutions

Tiago Rodrigues,[†] Carolina G. dos Santos,[†] Alessandra Riposati,[||] Leandro R. S. Barbosa,[§] Paolo Di Mascio,[‡] Rosangela Itri,[§] Maurício S. Baptista,[‡] Otaciro R. Nascimento,[||] and Iseli L. Nantes[†,*]

Centro Interdisciplinar de Investigação Bioquímica—CIIB, Universidade de Mogi das Cruzes—UMC, Mogi das Cruzes—SP, Brazil, Depto de Bioquímica, Instituto de Química, Universidade de São Paulo—USP, São Paulo—SP, Brazil, Instituto de Física, Universidade de São Paulo—USP, São Paulo—SP, Brazil, and Instituto de Física, Universidade de São Paulo—USP, São Carlos—SP, Brazil

Received: January 25, 2006; In Final Form: May 3, 2006

This work characterizes, for the first time, the photochemical behavior of the antipsychotic drugs thioridazine (TR), trifluoperazine (TFP), and fluphenazine (FP) influenced by the aggregation state of the molecules. Samples of monomeric and aggregated forms of phenothiazines were submitted to 20 min of irradiation at 254 nm for intervals of 1, 5, 10, 15, 20, or 25 days. In high phenothiazine concentrations, the irradiation led to the appearance of absorbance bands in the visible region peaking at 633 nm for TR and 509 nm for FP and TFP. In the dark, at room temperature and at 4 °C, these bands disappeared, after ∼15 and ∼60 min, respectively, but reappeared after a new irradiation session. These visible bands were assigned to stable cation radicals that were characterized by direct EPR measurements and by flash photolysis. Photogenerated stable cation radicals in the phenothiazine aggregates at room temperature are formed probably due to the stacking of the thiazine phenyl moieties. For the monomeric forms of phenothiazines, the spectral changes observed during the irradiation suggested the formation of sulfoxide and hydroxylated derivates. Oxidized derivates were detected by mass spectrometry of the aggregated forms of phenothiazines (>100 μM) only in the samples irradiated for more than 20 days. In contrast, monomeric phenothiazines were totally converted to the oxidized forms after 20 min of irradiation. Surface tension measurements of phenothiazines revealed that, in concentrations above 100 μM, the drugs formed aggregates. In the case of TR, small-angle X-ray scattering measurements indicated that this compound forms large lamellar-like aggregates in aqueous solutions.

Introduction

Phenothiazine derivatives have been the focus of several biological, chemical, physical-chemical, and photochemical studies due to their pharmaceutical properties and applications.[1,2] Particularly, the photochemical behavior of phenothiazines has gained interest as the compounds containing a phenothiazine moiety may promote photosensitizing effects in patients under therapy with these drugs.[3,4]

Literature data reveal that the photophysics and photochemistry of phenothiazine compounds are influenced by the substituents at positions 1 and 2 (Chart 1), the nature of the solvent, and the excitation energy.[5,6]

Under irradiation, phenothiazines can attain the first singlet excited state S_1 or S_n, depending on the energy of excitation and the solvent.[7] The formation of the singlet excited state S_n can occur by a biphotonic or a monophotonic absorption process. The decay of the singlet excited states can occur via internal conversion ($S_n \rightarrow S_1$ and $S_1 \rightarrow S_0$ plus heat), fluorescence ($S_1 \rightarrow S_0$ plus $h\nu$), and intersystem crossing ($S_1 \rightarrow T_1$ or $S_2 \rightarrow T_2$ and $T_2 \rightarrow T_1$, via internal conversion). The decay of the first triplet excited state can occur via phosphorescence. Phenothiazine derivates show comparatively weak values of quantum yields of fluorescence, but their quantum yields of phosphorescence are always better than 0.3 and sometimes very near 1. Therefore, it can be deduced that the quantum yields of the intersystem crossing (IC) for phenothiazine derivates are very near 1.[8] Besides the phosphorescence, two mechanisms can also answer for the triplet-state deactivation: energy transfer to molecular oxygen, which leads to the generation of $^1O_2$ (singlet molecular oxygen), and photoionization processes. The photoionization of phenothiazine derivates (PTH) could generate the cation radical and solvated electron (eq 1) or the neutral phenothiazine and hydrogen radicals (eqs 2 and 3).

$$\mathrm{PTH} \xrightarrow{h\nu} \mathrm{PTH}^* \rightarrow \mathrm{PTH}^{\bullet+} + \mathrm{e}^-_{\mathrm{s}} \quad (1)$$

$$\mathrm{PTH} \xrightarrow{h\nu} \mathrm{PTH}^* \rightarrow \mathrm{PT}^\bullet + \mathrm{H}^\bullet \quad \text{(monophotonic homolytic cleavage)} \quad (2)$$

$$\mathrm{PTH} \xrightarrow{h\nu} \mathrm{PTH}^* \rightarrow \mathrm{PTH}^{\bullet+} + \mathrm{e}^-_{\mathrm{s}} \rightarrow \mathrm{PT}^\bullet + \mathrm{H}^\bullet \quad \text{(thermal or photolytic deprotonation of } \mathrm{PTH}^{\bullet+}) \quad (3)$$

The photoionization of phenothiazines via the singlet manifold, yielding the cation radical, in competition with intersystem crossing and bond cleavage, has been described by several authors.[7,9,10] The cation radical can react with molecular oxygen, generating a phenothiazine sulfoxide derivate.[11]

The ability of some phenothiazine derivates to aggregate in micellar structures has been presented in the literature.[12]

* To whom correspondence should be addressed. Phone: +55-11-4798-7103. Fax: +55-11-4798-7102. E-mail: ilnantes@umc.br.
[†] Universidade de Mogi das Cruzes.
[‡] Instituto de Química, Universidade de São Paulo.
[§] Instituto de Física, Universidade de São Paulo—USP, São Paulo.
[||] Instituto de Física, Universidade de São Paulo—USP, São Carlos.

10.1021/jp0605404 CCC: $33.50
Published on Web 06/08/2006

CHART 1: Structure of Phenothiazine Compounds

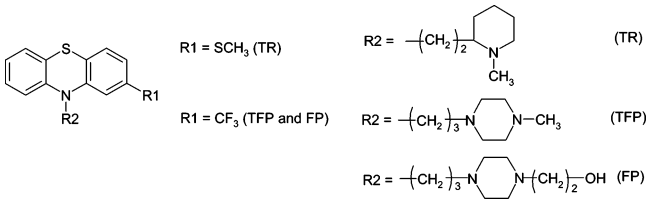

However, there is not a systematic study correlating the photophysics and photochemistry of phenothiazines with their aggregation state. In this work we present a comparative study of the photophysics and photochemistry of three phenothiazine derivates in the monomeric and aggregated states.

Materials and Methods

Chemicals. Trifluoperazine (TFP), thioridazine (TR), fluphenazine (FP), and SDS were obtained from Sigma Chemical Co. (St. Louis, MO). All aqueous solutions were prepared with deionized water (mixed bed of ion exchanger, Millipore), and the pH was measured using a combined glass electrode (Orion Glass pH SURE-FLOW). The reference electrode (ROSS, model 8102) was filled with Orion filling solution (ROSS). The pH meter was calibrated using METREPAK pHydrion standard buffer solutions (Brooklyn, NY).

Preparation of Phenothiazine and SDS Micellar Solutions. Phenothiazine and SDS micellar solutions were prepared by dissolving the surfactants in an appropriate buffer with stirring at 37 °C. The cmc (critical micelle concentration) of phenothiazines was determined in the usual fashion from plots of the surface tension vs log [surfactants]. Surface tensions were measured with a DeNoüy tensiometer equipped with a Pt ring.

Electronic Absorption Spectrometry. Electronic absorption measurements of cytochrome *c* were conducted in a photodiode spectrophotometer (Shimadzu Scientific Instruments Inc., Columbia, MD), by using quartz cuvettes of 1.0 or 0.1 cm light path and a slit of 0.5 nm.

EPR Spectrometry. Direct EPR measurements of phenothiazines were taken using an EPR Varian E-109, X-band system. The measuring conditions were gain 5×10^3, modulation amplitude 0.01 mT, microwave power 5 mW, and time constant 0.064 ms, equipped with room made digital detection. The temperature, magnetic field running, and microwave frequency are indicated in the EPR figure captions.

The calculation of the radical concentration was done by using the area of the EPR spectra of the standard KCl PITCH (Varian) with $g = 2.0026$ and whose signal intensity corresponds to 3.0×10^{15} spins/cm of sample in the cavity. In our conditions the total number of spins that generate the EPR signal corresponds to 6.9×10^{15} spins. The EPR signals of PITCH and phenothiazines were integrated and corrected according to the gain and microwave power.

SAXS (Small-Angle X-ray Scattering) Measurements. Considering that, in high concentrations, the drugs decreased significantly the medium pH (pH $\approx$ 5.0 for TR, and pH $\approx$ 3.5 for TFP and FP), for SAXS measurements the pH was adjusted to 4.0. Aqueous solutions containing 5 and 25 mM TFP, TR, and FP (pH 4.0) were placed in a 1 mm thick mica cell, positioned perpendicular to the incident X-ray beam at the SAXS beam line of the National Laboratory of Synchrotron Light (LNLS; Campinas, Brazil). The samples were studied at a room temperature of 22 $\pm$ 1 °C, with a radiation wavelength λ of 1.608 Å and a sample-to-detector distance of ~600 mm. A one-dimensional position-sensitive detector was used. SAXS curves were obtained with an acquisition time of 15 min.

SAXS data were collected in the range $0.007\ \text{Å}^{-1} < q < 0.35\ \text{Å}^{-1}$ ($q = (4\pi \sin\theta)/\lambda$ is the scattering vector; 2θ is the scattering angle).

The scattered intensity was corrected for the aqueous solution scattering taking into account the sample's attenuation factor and detector homogeneity. It is well-known that the intensity $I(q)$ from a set of scattering particles of volume V and electron density $\rho(r)$, randomly distributed in a solution of electron density ρ_0, is proportional to the number of scattering particles and V^2 as well as to $(\Delta\rho(r))^2$, where $\Delta\rho(r) = \rho(r) - \rho_0$. In the absence of interparticle interference effects, $I(q)$ can be written as a Fourier transform of the pair distance distribution function, $p(r)$, the probability of finding a pair of small elements at a distance r within the entire volume of the scattering particle as[13,14]

$$I(q) = (4\pi)\int_0^{D_{\max}} p(r)\frac{\sin(qr)}{qr}\,\mathrm{d}r \qquad (4)$$

where $p(r) = r^2\Delta\rho^2(r)$; $\Delta\rho^2(r)$ is the convolution square of the scattering density contrast $\Delta\rho(r)$ averaged over all directions in space. $D_{\max}$ is the particle maximum dimension in such a way that $p(r)$ goes to zero for $r \geq D_{\max}$. In addition, $p(r)$ carries information about the scattering particle shape. In this work, the $p(r)$ function is obtained through indirect Fourier transformation of the SAXS curve by making use of the method developed by O. Glatter (generalized indirect Fourier transformation, GIFT, program)[15] followed by a deconvolution technique (Decon), also developed by Glatter,[16] which allows one to get information about $\Delta\rho(r)$. Thus, for a particle with certain symmetry, $p(r)$ is given by[16]

$$p_d(r) = r^{d-1}\Delta\rho_d{}^2(r) \qquad (5)$$

where d is 1, 2, or 3 for the electron scattering density at a normal distance from the lamella plane, from the cylinder axis, or from the center of the sphere, respectively. It should be remarked that, for $d = 1$ and $d = 2$, the model implicitly assumes that the scattering particles are elongated in two dimensions and one dimension, respectively. This means that the cross-section is quite smaller than the length of the whole particle for rodlike particles, in such a way that the SAXS experiment just allows us to access the information regarding the cylinder cross-section. In the case of a flat lamella, $d = 1$, the two dimensions of the plane are quite larger than its thickness. In this way, just information related to the lamellar thickness is retrieved from the SAXS curve.

Accordingly, for a chosen particle geometry, $\rho(r)$ is calculated by a deconvolution square-root method (Decon program; for details, see ref 16). The latter generates the $\rho(r)$ function correlated with a $p(r)$ which best agrees with that generated by the GIFT program. If the chosen particle symmetry deviates from the actual one, the $p(r)$ function is a poor approximation of the input GIFT's $p(r)$ function.[16]

Matrix-Assisted Laser Desorption Ionization (MALDI) Time-of-Flight (ToF) Mass Spectrometry. The MALDI-ToF MS analyses were performed using an Ettan MALDI-ToF Pro system equipped with a quadratic-field reflectron and a timed ion gate. Phonothiazine sulfoxide identification was conducted in reflectron mode with positive ionization at 20 kV. The sample was, in this case, mixed with equal volumes of 50% acenitrile and 0.5% trifluoracetic acid saturated with α-cyano-4-hydroxy-

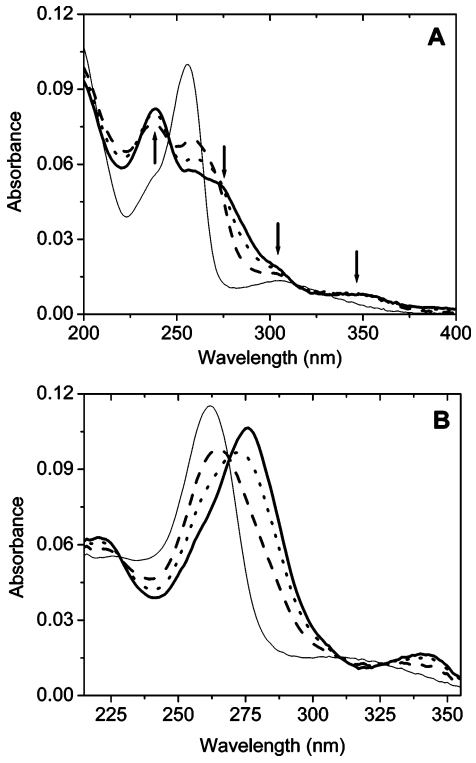

Figure 1. Spectral changes detected during the irradiation of 5 μM TFP (A) at times of zero (thin solid line), 0.5 min (dashed line), 1 min (dotted line), and 10 min (thick solid line) and TR (B) at times of zero (thin solid line), 0.5 min (dashed line), 1 min (dotted line), and 10 min (thick solid line). The samples were irradiated at 30 °C with a 4 W UV lamp at 254 nm. In panel A, the arrows indicate the peaks corresponding to the spectrum of the sulfoxide derivate.

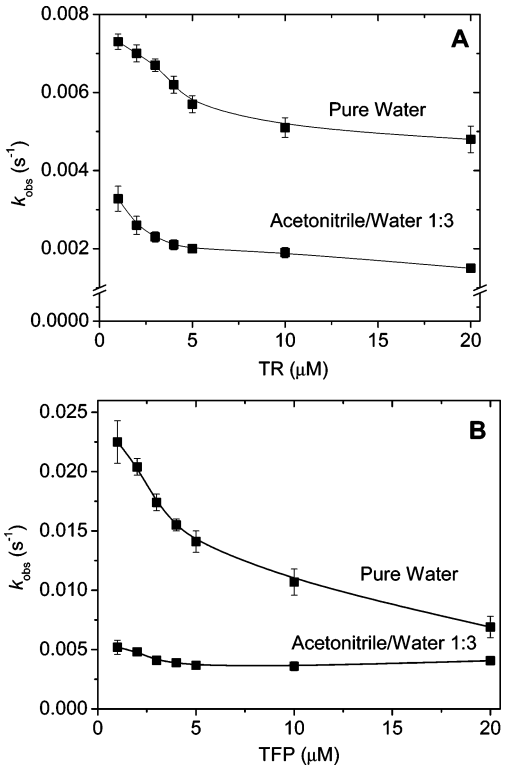

Figure 2. Changes in the rate of the formation of oxidized derivates of TR (A) and TFP (B) observed in pure water (pH 6.0) and an acetonitrile/water mixture (1:3) as a function of phenothiazine concentrations. The irradiation was carried out at 30 °C with a 4 W UV lamp for 10 min.

cinnamic acid. The data were analyzed using the Ettan MALDI-ToF Pro software system.

Results and Discussion

The irradiation of solutions of 5 μM TFP (Figure 1A), FP (not shown), and TR (Figure 1B) with a 4 W UV lamp at 254 nm for 10 min in buffered solutions at pH 4.0 and in pure water solutions (pH $\approx$ 6.0) led to spectral changes of the drugs that suggest the formation of the corresponding sulfoxide derivates.[11] The presence of isosbestic points at 246 nm for TFP (Figure 1A) and FP (not shown) suggested first-order kinetics. The spectral changes in TFP shown in Figure 1A are indicative of the sulfoxide formation due to the increase of the absorbance intensity at 230, 273, 302, and 348 nm as indicated by the arrows.[17] In contrast, the spectral changes observed for TR exhibited two isosbestic points at 228 and 269 nm, indicating second-order kinetics related to the formation of two products. Considering that the mass spectrometry of the photoproducts revealed an increase of 16 mass units relative to the TR mass (mass spectra not shown), it is probable that the sulfoxide and the derivate with the hydroxylated ring were the photoproducts generated by the UV irradiation. In this regard, it is expected that both of the products have the same mass. In fact, literature data reveal that shorter side chains in the structure of phenothiazines can favor radical dimerization, leading to hydroxylation regardless of the presence of external nucleophiles.[18] The reaction path to the formation of TR photoproducts is not the scope of the present work but deserves further investigations in the future.

The effect of the drug concentration and medium polarity on the rate of oxidized derivate formation was investigated for TR, TFP, and FP. The apparent rate constant for photochemically generated phenothiazine derivates was measured as a function of phenothiazine concentration, in pure water and in a 1:3 acetonitrile/water mixture (parts A and B of Figure 2 for TR and TFP, respectively). FP exhibited results similar to those of TFP (not shown). In the concentration range of 1−20 μM the drugs did not significantly lower the medium pH, which remained at ~6.0.

Figure 2 shows that the rate of oxidized photoproduct formation decreased with the increase of the phenothiazine concentration probably due to the formation of phenothiazine aggregates. On the other hand, the formation of oxidized photoproducts was also impaired in low-polarity media, acetonitrile/water mixtures (Figure 2), SDS micelles (not shown), and phospholipid liposomes (not shown). This effect was expected as the low-polarity media favor the neutral form of the radical. At this point, it is important to consider the mechanism of sulfoxide formation. Literature data have shown that phenothiazine-oxidized derivates are formed from the reaction of the cation radical with molecular oxygen, so conditions that favored the formation of the neutral radical could impair the formation of these derivates.[19] Literature data have also excluded the participation of $^1O_2$ in the photooxidation process, since the presence of $^1O_2$ quenchers does not modify the rate of sulfoxide formation.[19] This statement was corroborated in our conditions for the photooxidation of TR, TFP, and FP since the rates of the respective sulfoxide formation were similar in water and in deutered water (not shown).

The irradiation of TR, TFP, and FP in concentrations higher than 100 μM did not lead to spectral changes suggestive of sulfoxide formation. In this condition, even in an aerated medium, the appearance of an absorbance band in the visible region peaking at 633 nm for TR (Figure 3A) and 509 nm for

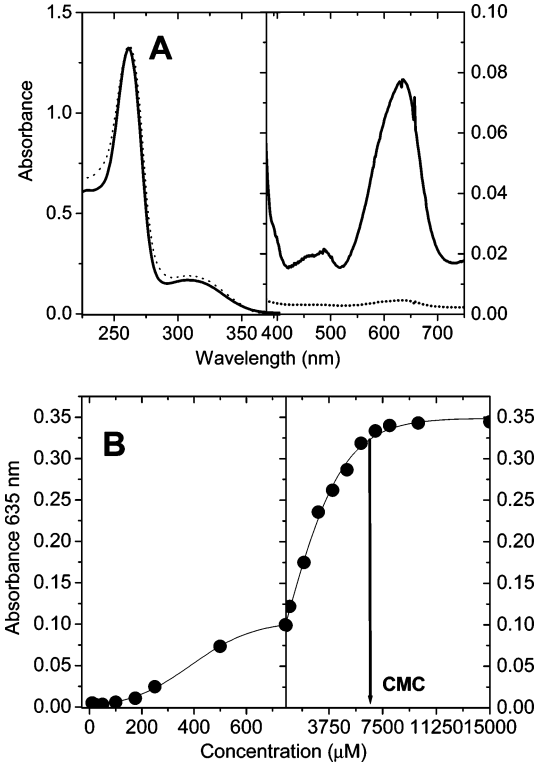

Figure 3. Spectroscopica behavior of the TR cation radical. (A) UV−vis spectrum of 5 mM TR obtained before (dotted line) and after (solid line) 10 min of irradiation with a 4 W UV lamp. The spectra shown in the left panel were obtained with a 0.1 cm optical path cuvette, and the spectra shown in the right panel were obtained with a 1.0 cm optical path cuvette. (B) Intensity of absorbance at 635 nm as a function of TR concentration. The irradiation was carried out at 30 °C with a 4 W UV lamp for 10 min.

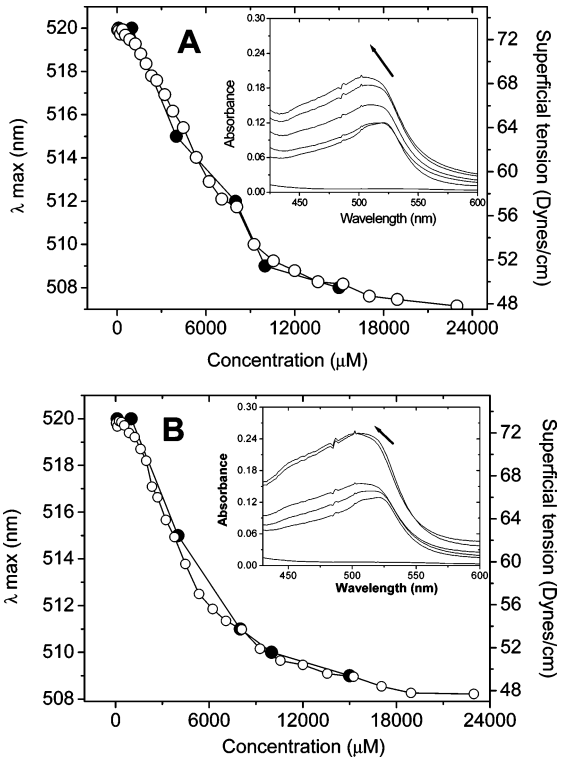

Figure 4. Effect of FP (A) and TFP (B) concentration on the wavelength of maximal absorption of the corresponding cation radical (closed circles) and on the superficial tension (open circles). The insets show the spectral changes exhibited by FP (A) and TFP (B) in the visible region as a function of the phenothiazine concentrations. The irradiation was carried out at 30 °C with a 4 W UV lamp for 10 min.

FP and TFP (shown in the inset of Figure 4, as can see below) was observed. In the dark, at room temperature and at 4 °C, these bands disappeared, after ∼15 and ∼60 min, respectively, but reappeared after a new irradiation session.

These bands were assigned to a cation radical stabilized in aggregated forms of the drugs. The appearance of visible bands after the photoionization of phenothiazines occurs because the removal of one electron from the HOMO (highest occupied molecular orbital) produces a SOMO (solely occupied molecular orbital) and changes the penultimate highest occupied molecular orbital to a new HOMO, which allows a low-energy SOMO−HOMO transition.[20] The analysis of Figure 3A also reveals that the formation of the TR cation radical was not accompanied by significant changes in the UV spectrum of the drug. This result suggests that the aggregation and the photoionization did not induce significant alterations in the drug structure and consequently did not affect the transitions $S_0 \rightarrow S_1$ and $S_0 \rightarrow S_n$. The effect of phenothiazine aggregation on the formation of sulfoxide was also investigated by mass spectrometry. Samples of monomeric and aggregated forms of phenothiazines were submitted to 20 min of UV irradiation with a 4 W UV lamp at 254 or 365 nm in an acid-buffered medium for intervals of 1, 5, 10, 15, 20, and 25 days. Mass spectrometry of the aggregated forms of phenothiazines (>100 μM) showed that significant concentrations of the oxidized derivates were present only in the samples irradiated during 20 and 25 days (not shown). In contrast, monomeric phenothiazines were totally converted to the oxidized forms after only one 20 min irradiation session (not shown). This result is also according to the proposal of stabilization of the phenothiazine cation radicals in their aggregate forms.

As expected, the intensity of the photochemically generated visible bands of TR did not obey the Lambert−Beer law as the stabilization of the cation radical should be favored by the formation of aggregates of the drug (Figure 3B). At first glance, the curve of absorbance intensity at 633 nm versus TR concentration seemed to exhibit a hyperbolic quadratic profile, but the expansion of the scale (Figure 3B, left panel) revealed a sigmoidal profile at low concentrations (below 500 μM). Probably, at low concentrations, it was difficult to aggregate two TR monomers, but once the dimers were formed, they acted as a nucleus on which other TR monomers could be easily associated. This result suggests a cooperative behavior for the aggregation of TR molecules. Figure 3B, right panel, shows also that the saturation was attained at the probable TR cmc determined by superficial tension measurements. This photochemical behavior of TR suggests that two types of TR aggregates could be formed and the cation radical stabilization was favored in the smaller aggregates. Therefore, below the TR cmc, an equilibrium between the TR monomer and TR small aggregates was established. The increase of the TR concentration led to the increase of the number of small aggregates and the corresponding increase of the absorbance at 633 nm. The saturation occurred probably because the number of TR molecules that can be stabilized in the cation radical form in a TR large aggregate is significantly lower than that stabilized in a small aggregate. Therefore, the number of cation radicals remained practically unchanged, as the equilibrium was dislocated to the large TR aggregates in concentrations above the cmc. Peculiar spectroscopical behavior as a function of concentration was exhibited by FP and TFP as the increase of the absorbance of the visible bands was accompanied by a blue shift of these bands (insets of Figure 4). By using the ϵ value

described in the literature (6538 $M^{-1}\cdot cm^{-1}$),[21] the yield of the TFP cation radical was estimated to be 0.6% for a sample of 5 mM TFP and 0.3% for a sample of 15 mM TFP. This is a rough estimate since an aggregate chromophore does not obey Beer's law. The differences in the cation radical yield according to the drug concentration were also observed by EPR and will be discussed below. However, the estimated yield of the cation radical calculated from the UV−vis spectra was close to that calculated by EPR measurements.

The plot of the maximal λ of TFP and FP visible bands as a function of the concentration of the drugs matched exactly with the corresponding plot of the superficial tension decrease versus the concentration of the drugs (Figure 4). Probably, for these drugs, the higher the number of TFP and FP molecules in an aggregate the more a specific arrangement of these molecules was favored. In fact, the X-ray structure of TFP (not shown[22]) reveals a lateral displacement of the TFP tail. This molecular structure is also expected for FP but not for TR, whose tail is considerably shorter. An interesting result was obtained when equal amounts of photochemically colored TR and FP or TFP were mixed, maintaining or not the concentration of both drugs above the determined cmc. In these conditions, the color (red) and visible bands of FP or TFP disappeared but the color (blue) and visible band of TR were preserved (not shown). All three studied drugs lost the photochemically acquired color when mixed with SDS micelles (not shown). Thus, TR aggregates seem to be more stable than TFP and FP aggregates. In the presence of TR aggregates, probably the aggregates of TFP and FP fall apart and the monomers are dispersed in the TR aggregates.

The aggregates of TR, TFP, and FP were analyzed by SAXS. Scattering was not observed for aqueous solutions of 5 mM TFP, TR, and FP, i.e., below the drug cmc according to Figure 3B. This result could be attributed to a small number of aggregates unable to produce a detectable signal under our experimental conditions. Samples containing 25 mM TFP and FP did not show any significant small-angle scattering, unlike the sample of 25 mM TR. Such a finding reveals that, at pH 4.0, although the hydrophobic contribution must play a role in the self-assembly process, the electrostatic interaction of TFP and FP molecules must preclude the formation of large aggregates since no salt was added to the solution. Interestingly, the sample containing 25 mM TR presents a nice scattering curve (opened circles), as displayed in Figure 5A.

First of all, we try to fit the data by supposing spherical and cylindrical-like aggregates, without satisfactory results. On the other hand, Figure 5B exhibits the $p_t(r)$ function obtained from the SAXS curve with the assumption of planar symmetry for the aggregates, where $p_t(r)$ corresponds to the distance distribution function along the lamella thickness ($d = 1$ in eq 2), associated with the electron density distribution $\rho(r)$ (inset) at the normal distance from the flat lamella plane ($\rho_0 = \rho_{water}$ corresponds to the zero level). Figure 5A shows the corresponding theoretical scattering modeling (thick line). Figure 5A shows that there is a good agreement between the observed and the modeling curves, indicating that the TR molecules form very large lamellar-like aggregates in aqueous solution at pH 4.0. Indeed, the scattering curve at low q values decays as q^{-2}, which is also a fingerprint of the scattering of flat lamella-like particles.[16] The combined results of $p_t(r)$ and $\rho_t(r)$ provide evidence that the lamellar thickness is on the order of 32 ± 2 Å and is made up of two shells of distinct electron densities in relation to the water electron density. This result must correspond to an arrangement of the TR molecules in a parallel

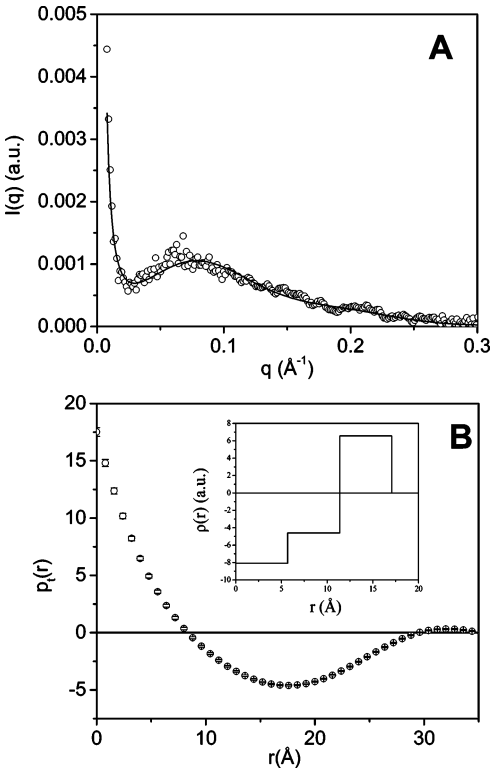

Figure 5. (A) Scattering curve (open circles) produced by 25 mM TR in water at pH 4.0. (B) $p_t(r)$ function obtained from the SAXS curve with the assumption of planar symmetry for the aggregates, where $p_t(r)$ and $\rho(r)$ correspond, respectively, to distance distribution and electron distribution functions along the lamella thickness ($d = 1$ in eq 2), resulting in a theoretical scattering curve that is represented as a thick line in (A).

CHART 2: Bidimensional Presentation of Two Possible Self-Assembies of TR Molecules in High Molar Concentrations

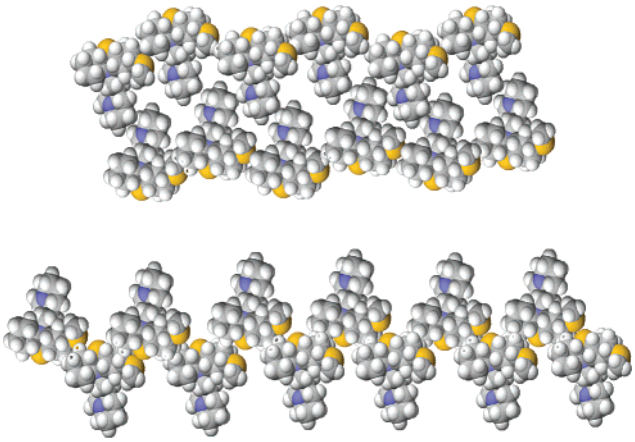

double layer with the phenothiazinic rings at the lamella surface and the tails confluent toward the inner lamella structure[22] (Chart 2, up). Such self-assembly of TR molecules is similar to that found for the molecules disposed in layers within its native crystallographic cell.[22] However, the possibility of a reverse bilayer structure could not be discarded (Chart 2, down). Thus, the exact topographic arrangement of the TR lamella-like aggregate remains to be elucidated. Furthermore, as we just have access to the lamella dimension normal to its surface, we cannot infer about the corresponding aggregation number of such a TR aggregate.

At this point it was important to characterize the excited state of these drugs in the aggregated forms. Transient decay spectra

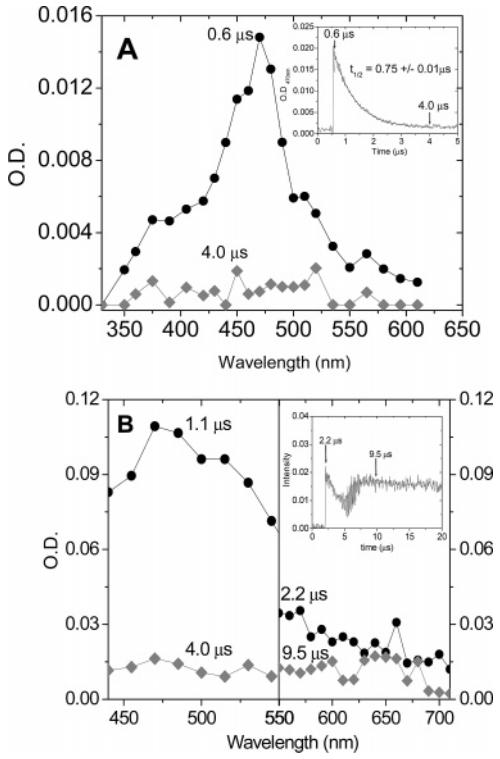

Figure 6. (A) Flash photolysis transient spectra of TR at a concentration of 200 μM obtained 0.6 and 4.0 μs after the laser pulse. The inset represents the kinetic profile at 470 nm, and the arrows indicate the times corresponding to the spectra (0.6 and 4.0 μs). (B) Flash photolysis transient spectra of TR at a concentration of 5 mM obtained 1.1 and 4.0 μs (left panel) and 2.2 and 9.5 μs (right panel) after the laser pulse. The inset represents the kinetic profile at 650 nm, and the arrows indicate the times corresponding to the spectra shown in the right panel (2.2 and 9.5 μs).

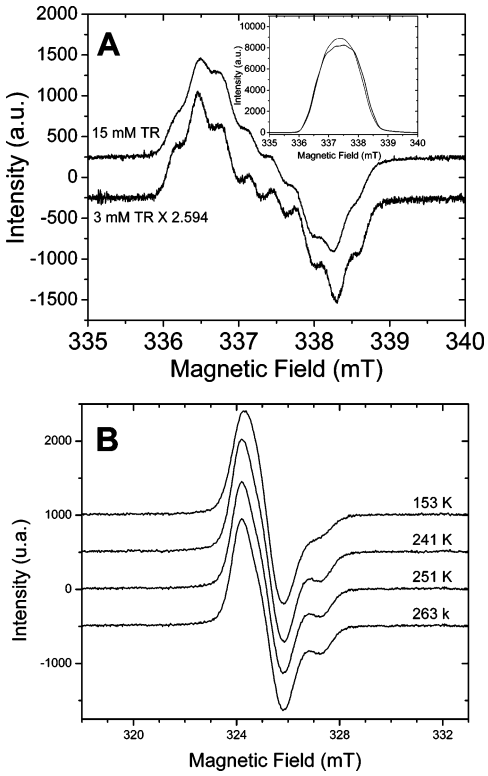

Figure 7. (A) EPR spectrum of 3 and 15 mM TR obtained at room temperature in H_2O (upper and lower solid lines) (frequency of the microwave 9.44079 GHz, scanning of the magnetic field 6.0 mT, modulation field 0.01 mT, microwave power 5 mW). (B) EPR spectrum of 5 mM TR obtained at different temperatures (modulation field 0.01 mT, microwave power 5 mW).

obtained from the laser photolysis of 200 μM and 5 mM TR, in an aerated medium, are shown in parts A and B of Figure 6, respectively.

For both TR concentrations (200 μM and 5 mM), the transient spectra obtained at the initial time, i.e., at 0.6 and 1.1 μs, respectively, contain the peaks for the TR triplet state at 470 nm that are shown in Figure 6A and the left panel of Figure 6B, respectively (black balls). Figure 6A and the left panel of Figure 6B show that the triplet transient signal decayed drastically after 4.0 μs (gray tilted squares). The inset of Figure 6A shows the decay of the triplet state in the presence of oxygen with a lifetime of 0.75 μs. In an argon atmosphere, the TR lifetime increased 200-fold. In the transient spectrum of 5 mM TR obtained at 9.5 μs, the transient absorption peak at 650 nm that is assigned to the TR cation radical is clearly seen (gray tilted squares in the right panel of Figure 6B). The inset of the right panel of Figure 6B shows the kinetic profile of the transient signals obtained at 650 nm (TR cation radical) and recorded ~2.2 μs after the laser pulse (see arrow). Note that the signal at 650 nm of 5 mM TR exhibits two components: the triplet decay and the radical formation, the last one not observed at 200 μM TR. The transient spectra of 200 μM and 5 mM TFP and FP are very similar (not shown). For TFP and FP the absence of oxygen increased the lifetime of the corresponding triplet species 10-fold. By knowing that the irradiation of TR, TFP, and FP aggregates generates a stable cation radical, EPR measurements of the photochemically colored drugs constitute an adequate technique to corroborate this proposal. If stable cation radicals of the studied phenothiazines could be generated, the EPR signal of these species should be obtained in the absence of spin-trapping molecules.

Figure 7A shows the EPR spectrum of TR at concentrations of 3 and 15 mM (thin and thick solid lines, respectively), obtained at a room temperature of 25 °C, after 10 min of irradiation with a UV lamp. The spectra show a hyperfine structure with eight lines.

The analysis of these spectra revealed that the lines are equally distant from each other but exhibit different intensity ratios. This result is compatible with the expected EPR spectrum of a large molecule in which a slow rotational correlation time could mix lines anisotropically distributed. The EPR spectrum of 3 mM TR was simulated with the SimFonia program (see Figure 1 in the Supporting Information) considering the existence of seven equivalent hydrogens (nuclear spin $I_H = 1/2$) and one nitrogen atom (nuclear spin $I_N = 1$), and the parameters obtained were $g_0 = 2.00525 \pm 0.00005$, $a_H = 0.29$ mT, and $a_N = 0.30$ mT. The simulated EPR spectrum reproduced the position of the lines of the experimental spectrum but not the intensity ratios of the peaks as the program considered a free radical with a fast rotational correlation time. The TR EPR spectra shown in Figure 7A and obtained at concentrations of 3 and 15 mM (small and large lamellar aggregates, respectively) show the following differences: (i) the signal intensity of the EPR spectrum obtained at 15 mM was ~2.5-fold higher than that obtained at 3 mM and not 5-fold as should be expected if only the number of aggregates was changed with the increase of the concentration; (ii) the EPR spectrum of the sample containing 15 mM TR exhibits a line width narrower than that obtained with 3 mM TR as attested by the different spectral absorptions (obtained by the numerical integration of the experimental spectra) shown in the inset. As commented before, this fact should be attributed

to a decrease in the stability of the cation radical or to less efficient photoexcitation in large aggregates. Also, in the large aggregates the spin−spin interaction could be responsible for the decrease of the line width and consequently the decrease of resolution of the hyperfine lines. Similar results were obtained for TFP at concentrations of 3 and 15 mM. Probably, antiferromagnetic spin−spin interaction of the irradiated samples of TR and TFP occurs since the EPR half-field signals (corresponding to $\Delta M_s = \pm 2$ coming from a ferromagnetic coupling and giving spin $S = 1$) were absent in the measurements, at 4.3 K. The yield of the cation radical was calculated by using the PITCH KCl standard (see the Materials and Methods) in comparison with EPR spectra of 10 mM TR and TFP. In this condition the calculations revealed a yield of 0.5% for TR and 1% for TFP, values close to those achieved from the UV−vis results.

Figure 7B shows the EPR experimental results obtained with TR over a temperature range from 263 to 153 K. As expected for a massive large molecule or aggregate the EPR spectrum did not exhibit the hyperfine lines even at 263 K. In this case, the hyperfine lines that became undetectable contribute to the broadening of the spectrum. The QPOW program was used to simulate the EPR spectrum of TR obtained at 153 K considering an unpaired electron that interacts with seven equivalent hydrogen nuclei and one nitrogen nucleus (see the results in the Supporting Information) The parameters obtained from the simulation were $A_{H,x} = 0.232$ mT, $A_{H,y} = 0.252$ mT, $A_{H,z} = 0.306$ mT, $A_{N,x} = 0.150$ mT, $A_{N,y} = 0.150$ mT, $A_{N,z} = 0.900$ mT, $g_x = 2.0131$, $g_y = 2.0059$, and $g_z = 1.9990$ with a Gaussian line shape. It is important to notice that a g_x value below 2 is compatible with a cation radical. These results also show that although the TR cation radical should be located in an aggregate as indicated by the slow rotational correlation time, the unpaired electron was not shared with other neighbor molecules.

The EPR spectra of TFP (Figure 8A) and FP (not shown) are similar. The high number of hyperfine lines exhibited by the EPR spectra of TFP and FP suggest an unpaired electron shared between two molecules. The second derivate of the EPR spectrum of TFP (Figure 8A) exhibits 27 lines corresponding to a dimeric free radical with 14 and 2 equivalent atoms of hydrogen and nitrogen, respectively.

The parameters obtained from the simulation were $g_0 = 2.00518 \pm 0.00005$, $a_H = 0.250$ mT, and $a_N = 0.363$ mT. Once more the simulation (dotted line) reproduced the position but not the form of the lines. This fact occurred because the experimental EPR spectrum was compatible with a large and massive molecule with a slow rotational correlation time. Figure 8B shows EPR experimental results obtained for TFP over a temperature range from 263 to 153 K. As expected for a massive large molecule or aggregate the EPR spectrum did not exhibit the hyperfine lines even at 263 K. In this case, the hyperfine lines that became undetectable contribute to the broadening of the spectrum. However, in this case, at 263 K the signals of two free radical spectra were evident. One of these signals could be attributed to an aggregate with a slow rotational correlation time as the hyperfine lines could not be observed at this temperature. The other signal at the region of the central field became well-defined at 268 K and could be attributed to a small molecule with a fast rotational correlation time. Because of the overlap of the signal of these two radicals, it was impossible to simulate the spectrum of the TFP cation radical at 153 K.

The stability of cation radicals in mild conditions has been previously described only for polymers whose molecular

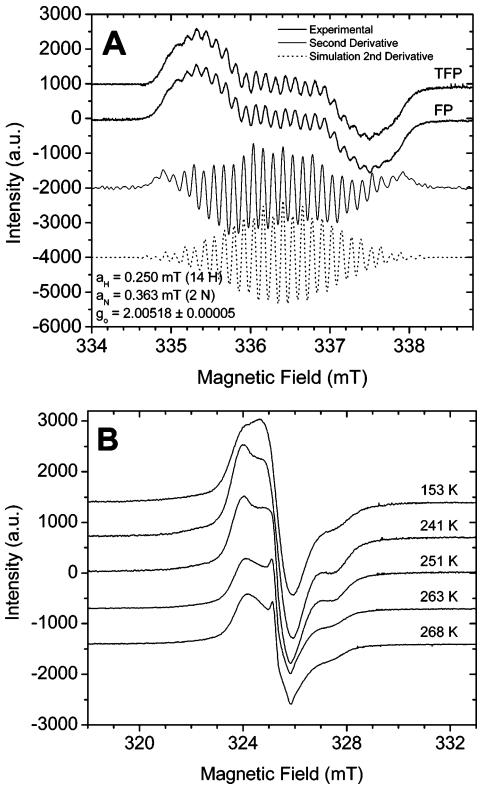

Figure 8. (A) EPR spectrum of 10 mM TFP and FP obtained at room temperature in H_2O (upper solid lines) and spectral simulation made by the program SimFonia da Bruker (low solid and dashed lines) (frequency of the microwave 9.44118 GHz, scanning of the magnetic field 6.0 mT, modulation field 0.01 mT, microwave power 5 mW. (B) EPR spectrum of 5 mM TFP obtained at different temperatures (frequency of the microwave 9.13384 GHz, magnetic field scanning 16.0 mT, modulation field 0.01 mT, microwave power 5 mW).

CHART 3: Different Structural Arrangements of Polyanilines: Poly-*p*-aniline (Left), Poly-*m*-*p*-aniline (Middle), and Poly-*m*-aniline (Right)

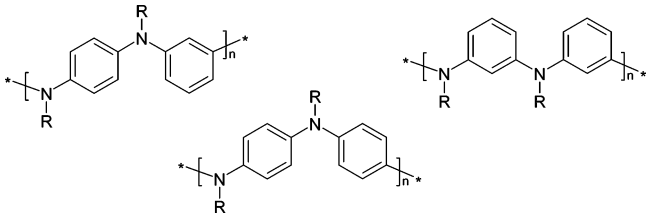

construction allows strong intramolecular spin coupling by holding radicals together.[23−33]

Concerning the present work, the polymers containing aniline units are models of the polaronic organic ferromagnet and are particularly interesting to consider. Some basic structures of polyaniline chains are shown in Chart 3. The oligo(cation radicals) of poly-*m*-*p*-aniline and poly-*m*-aniline exhibit a ground high-spin state and are stable at ambient temperatures.[32−35] In these molecules the structural similarity of the aniline units with the phenothiazine moieties is evident.

Surprisingly, in the studied phenothiazine aggregates, the cation radical stability was attained in the absence of covalent links between the spin-carrying units. McConnel[36] describes a model in which the intermolecular ferromagnetic coupling could be attained by a stack of radicals. In this model, atoms with positive spin densities establish interactions with atoms of neighboring radicals with small negative spin densities, leading to a ferromagnetic spin alignment of unpaired electrons of the different radicals. Experimentally this model has been observed

SCHEME 1: Photochemical Behavior of Phenothiazines Influenced by the Aggregation State of the Drugs

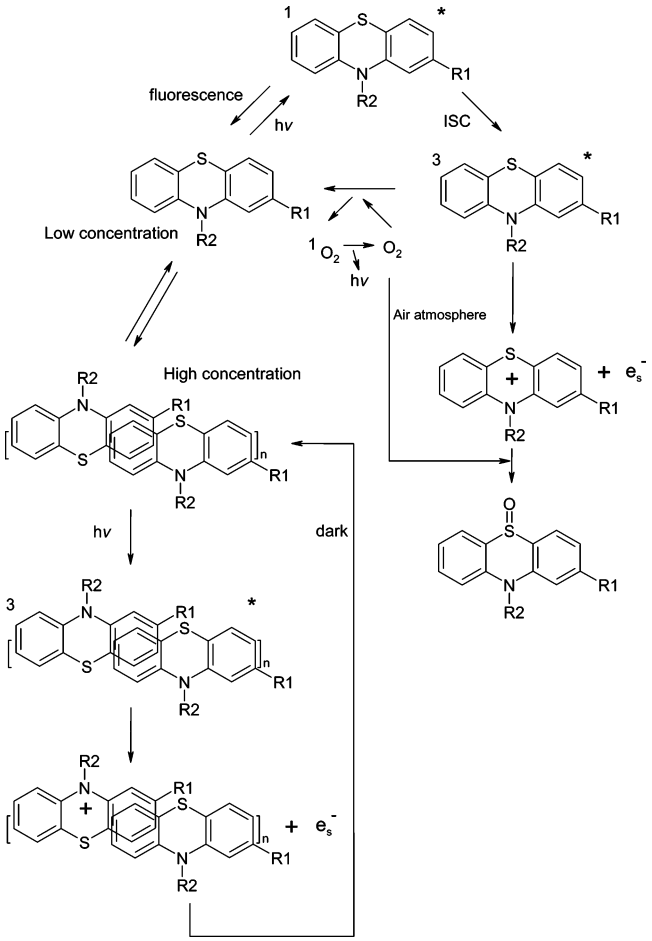

for [2.2]paracyclophanes substituted with two diphenylcarbenes.[37,38] This behavior could be rationalized by the application of the McConnell theory. However, in the case of the studied phenothiazines, no signal assignable to a triplet ground state of the cation radicals was detected by EPR (absence of the half-field signal in the EPR spectra) at 4 K. In the self-assembly model of stable cation radicals phase transition temperatures to the ferromagnetic phase could be extremely low (typically less than 1 K). Consequently, it is hard to elucidate the accurate mechanism of spin ordering in those organic ferromagnets.

Conclusion

The results described above led us to the following conclusions: (i) In the monomeric form, the triplet excited states of the investigated phenothiazines TR, TFP, and FP form the cation radicals that react with molecular oxygen, leading to the formation of the corresponding oxidized products. The formation of oxidized derivates was impaired in high drug concentrations and in low-polarity media due to the formation of drug aggregates and the neutral form of the drug-free radical, respectively. (ii) At high concentrations and in pure water, TR forms small and large lamellar aggregates characterized by SAXS and TFP and FP may form smaller aggregates. (iii) In the aggregate form, the triplet excited states of the investigated phenothiazines TR, TFP, and FP are able to form stable cation radicals at room temperature probably due to the stacking of the thiazine phenyl moieties. (iv) The photochemically generated cation radicals exhibit absorption visible bands due to a HOMO → SOMO transition. (v) In the aggregate form, the TR cation radical exhibits an unpaired electron centered only in one molecule and TFP and FP cation radicals exhibit an unpaired electron shared between two molecules of the drugs. The photochemical behavior of the investigated phenothiazines influenced by the aggregation state is summarized in Scheme 1.

Acknowledgment. We thank the Fundação de Amparo à Pesquisa do Estado de São Paulo (FAPESP), Conselho Nacional de Pesquisa (CNPq; Proc. 476119/2004-9 and CT-FVA/CNPq 01/2003 Proc. 400618/2004-4**)**, and Fundação de Amparo ao Ensino e Pesquisa da Universidade de Mogi das Cruzes (FAEP-UMC) for financial support. T.R. is a fellow of FAPESP, C.G.d.S. is a fellow of CNPq, and L.R.S.B is a fellow of CAPES (Coordenadoria de Aperfeiçoamento de Pessoal de Ensino Superior).

Supporting Information Available: EPR spectrum of 5 mM TR at room temperature and 153 K, with the corresponding simulated spectra. This material is available free of charge via the Internet at http://pubs.acs.org.

References and Notes

(1) Piette, J.; Decuyer, J.; Merville-Louis, M.-P.; Van de Vorst, A. *Biochimie* **1986**, *68*, 835−842.
(2) Zhelev, Z.; Ohba, H.; Bakalova, R.; Hadkimitova, V.; Ishikawa, M.; Shinohara, Y.; Baba, Y. *Cancer Chemother. Pharmacol.* **2004**, *53*, 267−275.
(3) Elisei, F.; Latterini, L.; Aloisi, G. G.; Mazzucato, U.; Viola, G.; Mioio, G.; Vedaldi, D.; Dall'Acqua, F. *Photochem. Photobiol*. **2002**, *75*, 11−21.
(4) Viola, G.; Latterini, L.; Vedaldi, D.; Aloisi, G. G.; Dall'Acqua, F.; Gabellini, N.; Elisei, F.; Barbafina, A. *Chem. Res. Toxicol.* **2003**, *16*, 644−651.
(5) Ortiz, A.; Poyato, I.; Fernández-Alonso, J. I. *J. Pharm. Sci.* **1983**, *72*, 50−55.
(6) Kelder, P. P.; De Mol, N. J.; Janssen, L. H. M. *Biochem. Pharmacol.* **1991**, *42*, 1551−1559.
(7) Ghosh, H. N.; Sapre, A. V.; Palit D. K.; Mittal, J. P. *J. Phys. Chem. B* **1997**, *101*, 2315−2320.
(8) Alkaitis, S. A.; Beck, G.; Gratzel, M. *J. Am. Chem. Soc.* **1975**, *20*, 5723−5729.
(9) Hall, R. D.; Buettner, G. R.; Chignell, C. F. *Photochem Photobiol.* **1991**, *54*, 167−173.
(10) Buettner, G. R.; Hall, R. D.; Chignell, C. F.; Motten A. G. *Photochem. Photobiol.* **1989**, *49*, 249−256.
(11) Galzigna, L.; Schiappelli, M. P, Scarpa, M, Rigo, A. *Free Radical Res.* **1997**, *27*, 501−504.
(12) Caetano, W.; Tabak, M. *J. Colloid Interface Sci.* **2000**, *225*, 69−81.
(13) Guinier, A., Fournet, G., Eds. *Small angle scattering of X-rays*; Wiley: New York, 1955.
(14) Glatter, O.; Kratky, O. *Small-angle X-ray scattering*; Academic Press: London, 1982.
(15) Glatter, O. *Acta Phys. Aust.* **1977**, *47*, 83−102.
(16) Glatter, O. J. *Appl. Crystallogr*. **1977**, *10*, 415−421.
(17) Davidson, A. G. *J. Pharm. Pharmacol.* **1977**, *28*, 795−800.
(18) Sackett, P. H.; Mayausky, J. S.; Smith, T.; Kalus, S.; McCreery, R. L. *J. Med. Chem.* **1981**, *24*, 1342−1347.
(19) Saucin, M.; Van de Vorst, A. *Radiat. Environ. Biophys.* **1980**, *17*, 159−168.
(20) Van Haare, J. A. E. H.; Van Boxtel, M.; Jansen, R. A. J. *J. Chem. Mater*. **1998**, *10*, 1166−1175.
(21) Vázquez, A.; Tudela, J.; Varón, R.; Garcia-Cánovas, F. *Anal. Biochem.* **1992**, *202*, 245−248.
(22) MacDowell, J. J. H. *Acta Crystallogr., B* **1977**, *31*, 2256.
(23) Iwamura, H. *J. Phys. Org. Chem.* **1998**, *11*, 299.
(24) Kahn, O. *Nature* **1995**, *378*, 667.
(25) Miller, J. S.; Calabrese, J. C.; Epstein, A. J.; Bigelow, R. W.; Zhang, J. H.; Reiff, W. M. *J. Chem. Soc., Chem. Commun.* **1986**, 1026−1028.
(26) Caneschi, A.; Gatteschi, D.; Laugier, J.; Rey, P. *J. Am. Chem. Soc.* **1987**, *109*, 2191−2194.
(27) Caneschi, A.; Gatteschi, D.; Laugier, J.; Rey, P.; Sessoli, R.; Zanchini, C. *J. Am. Chem. Soc.* **1988**, *110*, 2795.
(28) Caneschi, A.; Gatteschi, D.; Sessoli, R. *Acc. Chem. Res.* **1989**, *22*, 392−399.

(29) Chiarelli, R.; Novak, M. A.; Rassat, A.; Tholence, J. L. *Nature* **1993**, *363*, 147−148.

(30) Fukutome, H.; Takahashi, I.; Ozaki, M. *Chem. Phys. Lett.* **1987**, *133*, 34.

(31) Wienk, M. M.; Janssen, R. A. J. *J. Am. Chem. Soc.* **1997**, *119*, 4492−4501.

(32) Wienk, M. M.; Janssen, R. A. J. *Chem. Commun.* **1996**, *2*, 267−277.

(33) Wienk, M. M.; Janssen, R. A. J. *J. Am. Chem. Soc.* **1996**, *118*, 10626−10628.

(34) Stickley, K. R.; Selby, T. D.; Blackstock, S. C. *J. Org. Chem.* **1997**, *62*, 448−449.

(35) Wienk, M. M.; Janssen, R. A. J. *J. Am. Chem. Soc.* **1997**, *119*, 4492−4501.

(36) McConnell, H. M. *J. Chem. Phys.* **1963**, *39*, 1910.

(37) Izuoka, A.; Murata, S.; Sugawara, T.; Iwamura, H. *J. Am. Chem. Soc.* **1985**, *107*, 1784−1786.

(38) Izuoka, A.; Murata, S.; Sugawara, T.; Iwamura, H. *J. Am. Chem. Soc.* **1987**, *109*, 2631−2639.